Front. Phys. 13(5), 137803 (2018)
https://doi.org/10.1007/s11467-018-0779-x

RESEARCH ARTICLE

Wideband high-efficient linear polarization rotators

Zheng-Yong Song[1,†], **Qiong-Qiong Chu**[1], **Xiao-Peng Shen**[2,‡], **Qing Huo Liu**[3]

[1] *Institute of Electromagnetics and Acoustics, Department of Electronic Science, Xiamen University, Xiamen 361005, China*
[2] *School of Physical Science and Technology, China University of Mining and Technology, Xuzhou 221116, China*
[3] *Department of Electrical and Computer Engineering, Duke University, Durham, NC 27708, USA*
Corresponding authors. E-mail: [†] *zhysong@xmu.edu.cn,* [‡] *xpshen@cumt.edu.cn*
Received December 15, 2017; accepted March 14, 2018

We demonstrate a wideband polarization rotator with characteristics of high efficiency and large-range incidence angle by using a very simple anisotropic reflective metasurface. The calculated results show that reflection coefficient of cross polarization is larger than 71% over an octave frequency bandwidth from ∼4.9 GHz to ∼10.4 GHz. The proposed metasurface can still work very well even at incidence angle of 60°. The experiment at microwave frequencies is carried out and its results agree well with the simulated ones.

Keywords polarization, metasurface

PACS numbers 78.67.Pt, 78.20.-e

The arbitrary control of polarization states of electromagnetic (EM) waves is of great significance because of its wide applications in liquid crystal display, antenna radiation, spectroscopy, and optical instrumentation, which always attracts intense interest [1–18]. Various physical mechanisms to control polarization states from microwave to visible frequencies include wave plates, dichroic crystals, Brewster effects, Faraday materials, and birefringence of anisotropic materials, and so on [1, 2]. Some problems of conventional polarization-control materials, such as the bulky thickness of the structure, a narrow band, high losses, limited choice of materials, and the expensive price, are still deserved to be solved. Then there have been many attempts to develop new theories, technologies, and experiments to overcome these limitations. Recently, several different devices of polarization control are presented based on the concept of metamaterials (MMs) [3–21], which are artificial materials with unusual EM responses that are not unattainable with natural materials. So using MMs becomes highly desirable to design polarization control devices with high efficiency, large bandwidth, and sub-wavelength dimensions.

Recently, many metasurface-based phase engineered devices have been proposed for novel applications in wavefront manipulation [11], holography [12], and polarization control [13–18]. Yu *et al.* experimentally demonstrated optically thin quarter-wave plates built with plasmonic metasurfaces consisting of spatially varying phase and polarization responses [13]. Their design generates high-quality circularly polarized light with a high degree of circular polarization (> 0.97) for arbitrary orientation of the incident linear polarization from $\lambda = 5$ μm to 12 μm. Hao *et al.* proposed to use reflective anisotropic metasurfaces to manipulate polarization states of EM waves, and showed that a complete conversion between two perpendicular linear polarizations is realizable in the microwave frequency regime by experiment and simulation [14]. All possible polarizations (circular, elliptic, and linear) are realizable via adjusting material parameters in a narrow band. Grady *et al.* experimentally demonstrated ultrathin, broadband, and highly efficient MM-based terahertz polarization converters that are capable of rotating a linear polarization state into its orthogonal one [16]. Yang *et al.* experimentally presented an alternative approach to plasmonic metasurfaces by replacing the metallic resonators with dielectric meta-reflectarray for broadband linear polarization conversion with more than 98% conversion efficiency over a 200 nm bandwidth in the short-wavelength infrared band [18]. Replacing plasmonic nanoantennae with their dielectric counterparts allow loss to be largely reduced so as to cause increased efficiency. In this work, we propose an alternative structure of a wideband and wide-angle polarization rotator based on an artificially designed anisotropic metasurface [11–34], which is composed of one dimensional metallic grating placed on the top of a printed circuit board with a grounded metallic plane on the bottom.

In polarization optics, the key ingredient to control the states of polarization is to tailor the phase delay between two orthogonal optical axes. The designed metasurface introduces $\sim 180°$ phase difference between two orthogonal components of reflected wave. Polarization conversion has been presented by using such a thin anisotropic reflective metasurfaces from linearly-polarized wave to its cross-polarized wave. Both numerical and experimental results indicate that the proposed metasurface owns broadband operation with the polarization conversion coefficient larger than 71% from ~4.9 GHz to ~10.4 GHz. Moreover, the thickness of the designed system is only about $\sim \lambda/7$ at its center working wavelength which is potentially feasible for some applications where the space limitations are stringent, and takes favorable advantage of little energy loss. Meanwhile, when the incident wave is not polarized around 45° or 135°, the conversion ratio becomes very small which indicates that the proposed metasurface has a polarization selective performance.

As schematically shown in Fig. 1, the proposed wideband polarization conversion metasurface under study is composed of a layer of one dimensional metallic grating and a continuous grounded metallic film, and both of them are separated by a homogeneous printed circuit board (FR4) with the relative permittivity of $\varepsilon = 4.6+\mathrm{i}0.023$. Figure 1 gives the schematic of the designed [Fig. 1(a)] and fabricated [Fig. 1(b)] configurations. The width of metallic strips is sized 2.0 mm, and the periodicities of the array are 10.0 mm along x direction. The thicknesses of metallic strips, dielectric layer, and metallic film are 0.035 mm, 5.3 mm, and 0.035 mm. All materials are assumed to be non-magnetic ($\mu = \mu_0$). In our simulation, a unit cell is used with periodical boundary conditions assigned to approximate an infinite array along x direction, and the extremely fine mesh is adopted to discretize the space and ensure the convergence of the calculated results. Floquet ports are added on the top and bottom faces of the simulation domain to obtain reflection and transmission coefficients of a plane wave illuminating the structure at an arbitrary angle of incidence. The distance between the receiver and the designed structure is 200 mm, which is enough long so as to only get the propagating information of the reflected wave. Thus, the near-field effect of the reflected light is not included. Under normal incidence case or oblique incidence case, transverse electric (TE) wave with an incident angle θ can well satisfy the condition of the linearly polarized wave with electric field E_i only in the xy plane. Within prescribed polarization case, an incident plane wave with incident angle θ (between the z-axis and k) and polarization angle ϕ (formed by the x-axis and the projection of k on the xy plane) is illuminated on the deigned structure. As a result of the interaction between incident waves and the designed structure, the subsequent reflected wave typically includes co-polarized component $E_{//}$ (parallel to E_i) and cross-polarized component E_+ (perpendicular to E_i) due to the anisotropy of the meatsurface. In order to understand the principle of polarization conversion, the designed structure can be treated as a homogenous anisotropic MM layer with relative permittivity ε and dispersive relative permeability $\overleftrightarrow{\mu}$, which can be expressed by diagonal elements. The complex reflection coefficients associated with the polarization-dependent response of the structure can be analytically derived from a 4×4 transfer matrix model [14]. In our simulation, reflection coefficients of the co-polarized and cross-polarized waves are respectively defined as $r_{//}$ and r_+. Figure 2 illustrates the calculated reflection coefficient r_+ as red solid line under normal incidence case with polarization angle $\phi = 45°$ (or 135°) for E_i. Considering the normal incidence case ($\theta = 0°$), the direction definition of E_i is absolutely dependent on ϕ while the direction definition of wave vector k is completely independent of it. Obviously, the cross-polarized reflection coefficient is close to ~100% from ~6.0 GHz to ~10.0 GHz, demonstrating a 90° conversion of the linearly polarized wave after reflection and an outstanding half-powered bandwidth from ~4.9 GHz to ~10.4 GHz. The near perfect conversion band performs as an ideal pass-band filter and divides different polarizations into different frequency bands. Such a broadband polarization modulation demonstrated by our designed matedevice is hard to be achieved in natural crystal-based wave plates, which are restricted by the limitation of operating frequency and bandwidth on the thickness and dispersion. It is worth mentioning that the entire thickness of this metasurface is ~5.37 mm which is over 7 times less than the center working wavelength.

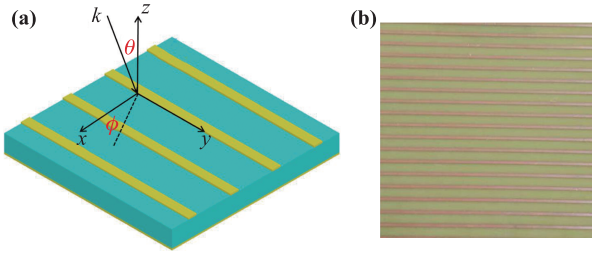

Fig. 1 **(a)** Three dimensional view of the geometry of the designed polarization rotator, which is composed of one dimensional metallic grating, an intermediate dielectric spacer, and a bottom continuous metallic layer. The yellow parts (strip and bottom layer) are metal modeled as copper, which can be treated as perfect electric conductor (PEC) in microwave region. The cyan part (spacer) is the 5.3 mm-thick substrate made of printed circuit board (FR4). **(b)** A top-view picture of part of the fabricated anisotropic reflective metasurface.

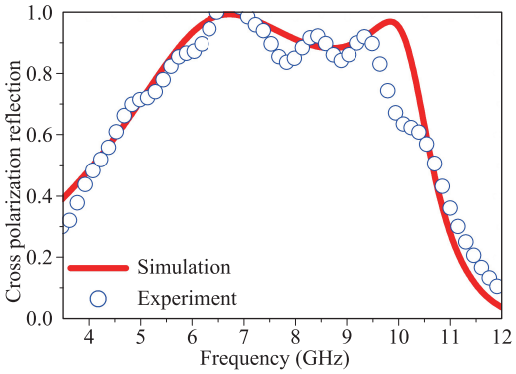

Fig. 2 Calculated (red solid line) and measured (blue hollow circle) reflection magnitudes of the cross-polarized r_+ waves with incident angle $\theta = 0°$ and polarization angle $\phi = 45°$ (or 135°).

To investigate the underlying physics behind this phenomenon, the intuitively interpreted mechanism of the designed system is shown in the inset of Fig. 3(a). It is assumed that a normally linear-polarized wave with polarization angle $\phi = 45°$ illuminates the metasurface, and its electric field $E_{\rm i}$ can be decomposed to two orthogonal electric field vector of $E_{{\rm i}x}$ and $E_{{\rm i}y}$. Also the electric field E_+ of the reflected wave can be decomposed into two independent polarizations of E_{+x} and E_{+y}, and the reflection amplitude (phase) for normally x-polarized and y-polarized incident components is defined as r_x and r_y (φ_x and φ_y). Then, polarization conversion as the role of a classical half-wavelength plate can be realized if coefficients of x-polarized and y-polarized components of the reflected waves are the same and the reflection phase difference for these two directions is $\sim 180°$. Figure 3 shows the amplitude and phase of reflection under normal incidence. It clearly tells that a nearly 100% reflection band for r_x and r_y are realized over the range of ~6.0 GHz to ~10.0 GHz providing the possibility of achieving high efficient polarization conversion. In fact, due to the existence of a continuous metal film with thickness 0.035 mm on the back, the entire system for EM waves is always completely reflective, independent of their incidence angles and polarizations. So it is easy to satisfy $r_x = r_y$. The calculated reflection phases (φ_x and φ_y) are illustrated in Fig. 3(b). We find in Fig. 3(c) that the phase difference $|\varphi_x - \varphi_y|$ between two reflection coefficients approaches $\sim 180°$ within wide spectral range 6.0–10.0 GHz, which is the key point to achieve wideband metasurface-enabled polarization conversions. Coincidentally, it is consistent with the frequency range where the r_+ peak is found in Fig. 2.

Furthermore, the dependence of cross polarization reflection r_+ of the proposed rotator on the thickness of dielectric layer is investigated. To briefly present this property, we only discuss cross polarization reflection

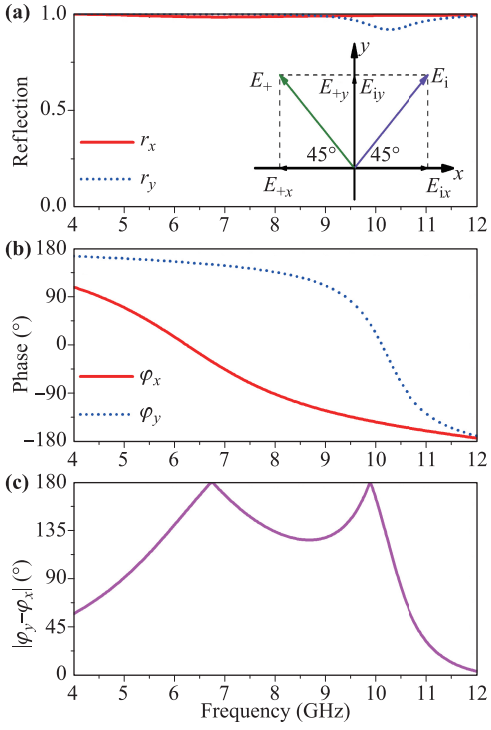

Fig. 3 Calculated reflection magnitudes **(a)** and reflection phases **(b)** for x-polarized (red line) and y-polarized (blue dot) waves on the designed metasurface for normally incident wave. Inset: An illustration of the working mechanism of the designed system. **(c)** Reflection phase difference $|\varphi_y - \varphi_x|$ as a function of frequency. There are two points of $|\varphi_y - \varphi_x|$ approaching to 180°, which corresponds to the two conversion extrema in Fig. 2.

under normal incidence. Figure 4 illustrates the relation between cross polarization reflection r_+ and the thickness of dielectric layer with other structure parameters unchanged. The calculated results tell that r_+ of the designed system under normal incidence is closely depend on the thickness of dielectric layer. As the thickness of dielectric layer increases from 1 mm to 7 mm, performance of r_+ firstly become improved and then a little worsened.

Based on above analyses, the designed polarization rotator is fabricated and measured in the microwave frequency. The proposed wideband polarization conversion metasurface is fabricated with a size of 500 mm × 500 mm. Figure 1(b) shows the photograph of the fabricated polarization rotator. In our experiments, the metasurface is shined by one horn antenna placed 50 cm away from the sample, and another identical horn antenna is used to receive the reflected signal. It should be noted that the center of the two linearly polarized horn antennas should be placed at the same height. By connecting them to an Agilent vector network analyzer via cables, both the magnitudes and phases of the reflected

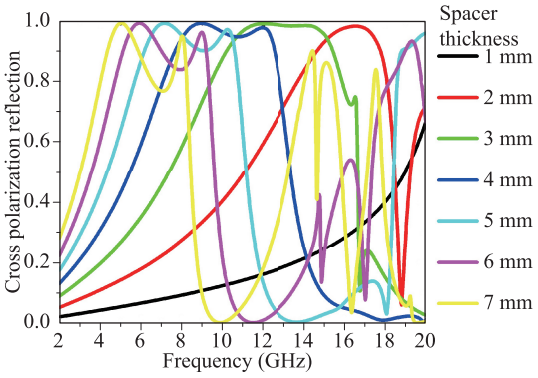

Fig. 4 Thickness dependence of cross polarization reflection r_+ under normal incidence with other structure parameters unchanged.

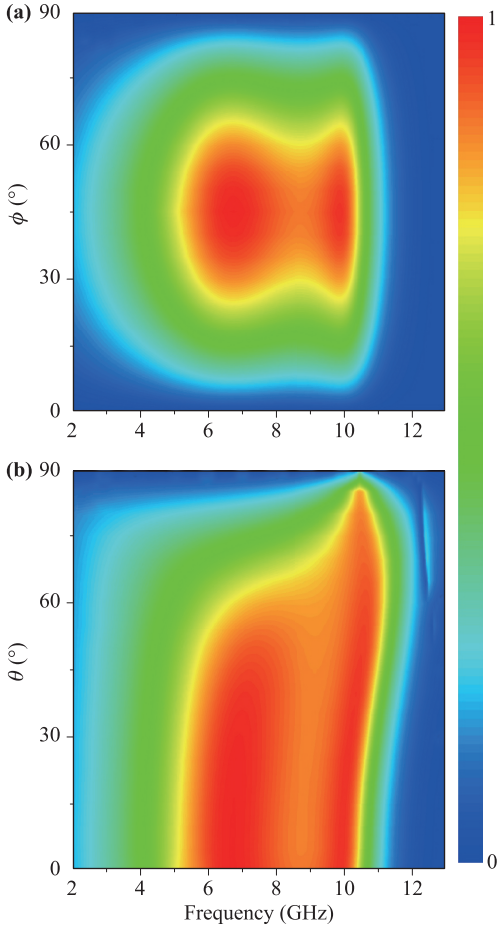

Fig. 5 **(a)** The variation of reflection coefficient r_+ with polarization angle (ϕ) and frequency (f) under the condition of incidence angle $\theta = 0°$. **(b)** The variation of reflection coefficient r_+ with θ and f under the condition of polarization angle $\phi = 135°$ in xy plane.

signals can be obtained. A copper plate with the same size has been measured for comparison in each experiment. When one of the two antennas is perpendicular to another, the cross-polarized reflection r_+ is measured. Through the comparison of available results, measurements (blue hollow circles in Fig. 2) are nearly consistent with simulations. Here are some main reasons which cause the difference between experiment and simulation: (i) uncertain factor and random error in the process of fabrication and measurement (shape, size, height, etc.); (ii) size of the whole sample is finite and not enough big; (iii) radiation of the horn antennas is not a perfect plane wave; (iv) measurements are performed at a small incident angle (10°); (v) the existence of oscillation is possibly due to multiple reflections between horn antennas.

To better understand polarization and angular dependence of this phenomenon, the numerically calculated reflectance r_+ is plotted in Fig. 5(a) as a function of polarization angle (ϕ) for E_i and frequency (f) with incidence angle $\theta = 0°$. With the anisotropy tuned on, r_+ could take a nonzero value, and the polarization conversion effect depends strongly on the polarization angle. When $\phi = 45°$ and $\theta = 0°$, reflection coefficient of polarization conversion r_+ is maximized. Different to that, we get $r_+ = 0$ under the condition of $\phi = 0°$ and $\phi = 90°$, indicating that polarization conversion effect vanishes. It looks very reasonable because of direction of normally incident $E(H)$ field is parallel to $x(y)$ coordinate axis when $\phi = 0°$, or direction of normally incident $E(H)$ field is parallel to $y(x)$ coordinate axis when $\phi = 90°$. To find out the dependence of the conversion performance on incident angle, we calculate the reflection coefficient r_+, depicted in Fig. 5(b), as a function of θ and f with $\phi = 45°$ for k and E_i along the polarization angle 135° in xy plane. The results in Fig. 5(b) are calculated in the TE case, where its E field is always in xy plane varying the incidence angle. At small incident angles, perfect polarization conversion is almost achieved in a wide frequency range of 6.0–10.0 GHz. When incident angle is increased larger than 60°, the conversion intensity presents a rapid decreasing trend, which clearly demonstrates the wide-angle operation characteristic of the proposed device. So it can provide great convenience in practical applications. This is beneficial because there is not necessary to strictly measure the sample under normal incidence, which is not easy to achieve in experiment.

In conclusion, we design a very simple anisotropic reflective metasurface to control polarization of EM waves in microwave frequency, and demonstrate that high-efficiency polarization rotator can be achieved by tailoring the spectral phase. The simulated and measured results are in good agreement, and both of them show that the proposed metasurface with a thin thickness can

efficiently achieve the polarization conversion in an octave frequency band. The advantages of the proposed polarization rotator are wide angle and high efficiency in a broad bandwidth. Therefore, this designed system is suitable for many potential applications in microwave instrumentation, wavefront manipulation, and polarization components.

Acknowledgements This work was supported by the National Natural Science Foundation of China (Grant Nos. 11504305 and 61372048).

References

1. M. Born and E. Wolf, Principles of Optics, Cambridge: Cambridge University Press, 1999
2. J. A. Kong, Electromagnetic Wave Theory, Cambridge: EMW Publishing, 2005
3. C. Huang, Y. Feng, J. Zhao, Z. Wang, and T. Jiang, Asymmetric electromagnetic wave transmission of linear polarization via polarization conversion through chiral metamaterial structures, *Phys. Rev. B* 85(19), 195131 (2012)
4. L. Feng, A. Mizrahi, S. Zamek, Z. Liu, V. Lomakin, and Y. Fainman, Metamaterials for enhanced polarization conversion in plasmonic excitation, *ACS Nano* 5(6), 5100 (2011)
5. R. Xia, X. Jing, X. Gui, Y. Tian, and Z. Hong, Broadband terahertz half-wave plate based on anisotropic polarization conversion metamaterials, *Opt. Mater. Express* 7(3), 977 (2017)
6. L. Y. Guo, M. H. Li, X. J. Huang, and H. L. Yang, Electric toroidal metamaterial for resonant transparency and circular cross-polarization conversion, *Appl. Phys. Lett.* 105(3), 033507 (2014)
7. J. Kaschke, L. Blume, L. Wu, M. Thiel, K. Bade, Z. Yang, and M. Wegener, A helical metamaterial for broadband circular polarization conversion, *Adv. Opt. Mater.* 3(10), 1411 (2015)
8. Y. Cheng, R. Gong, and L. Wu, Ultra-broadband linear polarization conversion via diode-like asymmetric transmission with composite metamaterial for terahertz waves, *Plasmonics* 12(4), 1113 (2017)
9. Y. Li, J. Zhang, H. Ma, J. Wang, Y. Pang, D. Feng, Z. Xu, and S. Qu, Microwave birefringent metamaterials for polarization conversion based on spoof surface plasmon polariton modes, *Sci. Rep.* 6(1), 34518 (2016)
10. M. Mutlu, A. E. Akosman, A. E. Serebryannikov, and E. Ozbay, Diodelike asymmetric transmission of linearly polarized waves using magnetoelectric coupling and electromagnetic wave tunneling, *Phys. Rev. Lett.* 108(21), 213905 (2012)
11. N. Yu, P. Genevet, M. A. Kats, F. Aieta, J. P. Tetienne, F. Capasso, and Z. Gaburro, Light propagation with phase discontinuities: Generalized laws of reflection and refraction, *Science* 334(6054), 333 (2011)
12. J. Lin, P. Genevet, M. A. Kats, N. Antoniou, and F. Capasso, Nanostructured holograms for broadband manipulation of vector beams, *Nano Lett.* 13(9), 4269 (2013)
13. N. Yu, F. Aieta, P. Genevet, M. A. Kats, Z. Gaburro, and F. Capasso, A broadband, background-free quarter-wave plate based on plasmonic metasurfaces, *Nano Lett.* 12(12), 6328 (2012)
14. J. M. Hao, Y. Yuan, L. X. Ran, T. Jiang, J. A. Kong, C. T. Chan, and L. Zhou, Manipulating electromagnetic wave polarizations by anisotropic metamaterials, *Phys. Rev. Lett.* 99(6), 063908 (2007)
15. Z. Y. Song, L. Zhang, and Q. H. Liu, High-efficiency broadband cross polarization converter for near-infrared light based on anisotropic plasmonic meta-surfaces, *Plasmonics* 11(1), 61 (2016)
16. N. K. Grady, J. E. Heyes, D. R. Chowdhury, Y. Zeng, M. T. Reiten, A. K. Azad, A. J. Taylor, D. A. R. Dalvit, and H. T. Chen, Terahertz metamaterials for linear polarization conversion and anomalous refraction, *Science* 340(6138), 1304 (2013)
17. Z. Y. Song, X. Li, J. M. Hao, S. Y. Xiao, M. Qiu, Q. He, S. J. Ma, and L. Zhou, Tailor the surface-wave properties of a plasmonic metal by a metamaterial capping, *Opt. Express* 21(15), 18178 (2013)
18. Y. M. Yang, W. Y. Wang, P. Moitra, I. I. Kravchenko, D. P. Briggs, and J. Valentine, Dielectric meta-reflectarray for broadband linear polarization conversion and optical vortex generation, *Nano Lett.* 14(3), 1394 (2014)
19. Z. Y. Song, and B. L. Zhang, Wide-angle polarization-insensitive transparency of a continuous opaque metal film for near-infrared light, *Opt. Express* 22(6), 6519 (2014)
20. Z. Y. Song, J. Zhu, C. Zhu, Z. Yu, and Q. H. Liu, Broadband cross polarization converter with unity efficiency for terahertz waves based on anisotropic dielectric meta-reflect arrays, *Mater. Lett.* 159, 269 (2015)
21. S. L. Sun, Q. He, S. Y. Xiao, Q. Xu, X. Li, and L. Zhou, Gradient-index meta-surfaces as a bridge linking propagating waves and surface waves, *Nat. Mater.* 11(5), 426 (2012)
22. P. C. Wu, W. Y. Tsai, W. T. Chen, Y. W. Huang, T. Y. Chen, J. W. Chen, C. Y. Liao, C. H. Chu, G. Sun, and D. P. Tsai, Versatile polarization generation with an aluminum plasmonic metasurface, *Nano Lett.* 17(1), 445 (2017)
23. P. C. Wu, W. Zhu, Z. X. Shen, P. H. J. Chong, W. Ser, D. P. Tsai, and A. Q. Liu, Broadband wide-angle multifunctional polarization converter via liquid-metal-based metasurface, *Adv. Opt. Mater.* 5(7), 1600938 (2017)

24. P. C. Wu, J. W. Chen, C. W. Yin, Y. C. Lai, T. L. Chung, C. Y. Liao, B. H. Chen, K. W. Lee, C. J. Chuang, C. M. Wang, and D. P. Tsai, Visible metasurfaces for on-chip polarimetry, *ACS Photonics*, (2017) (published soon)
25. P. C. Wu, N. Papasimakis, and D. P. Tsai, Self-affine graphene metasurfaces for tunable broadband absorption, *Phys. Rev. Appl.* 6(4), 044019 (2016)
26. L. Cong, P. Pitchappa, C. Lee, and R. Singh, Active phase transition via loss engineering in a terahertz MEMS metamaterial, *Adv. Mater.* 29(26), 1700733 (2017)
27. L. Cong, P. Pitchappa, Y. Wu, L. Ke, C. Lee, N. Singh, H. Yang, and R. Singh, Active multifunctional microelectromechanical system metadevices: Applications in polarization control, wavefront deflection, and holograms, *Adv. Opt. Mater.* 5(2), 1600716 (2017)
28. L. Cong, Y. K. Srivastava, and R. Singh, Near-field inductive coupling induced polarization control in metasurfaces, *Adv. Opt. Mater.* 4(6), 848 (2016)
29. L. Cong, Y. K. Srivastava, and R. Singh, Inter and intra-metamolecular interaction enabled broadband high-efficiency polarization control in metasurfaces, *Appl. Phys. Lett.* 108(1), 011110 (2016)
30. L. Cong, N. Xu, J. Han, W. Zhang, and R. Singh, A tunable dispersion-free terahertz metadevice with Pancharatnam-Berry-phase-enabled modulation and polarization control, *Adv. Mater.* 27(42), 6630 (2015)
31. L. Cong, N. Xu, W. Zhang, and R. Singh, Polarization control in terahertz metasurfaces with the lowest order rotational symmetry, *Adv. Opt. Mater.* 3(9), 1176 (2015)
32. L. Cong, W. Cao, X. Zhang, Z. Tian, J. Gu, R. Singh, J. Han, and W. Zhang, A perfect metamaterial polarization rotator, *Appl. Phys. Lett.* 103(17), 171107 (2013)
33. D. L. Markovich, A. Andryieuski, M. Zalkovskij, R. Malureanu, and A. V. Lavrinenko, Metamaterial polarization converter analysis: Limits of performance, *Appl. Phys. B* 112(2), 143 (2013)
34. R. Malureanu, W. Sun, M. Zalkovskij, Q. He, L. Zhou, P. Uhd Jepsen, and A. Lavrinenko, Metamaterial-based design for a half-wavelength plate in the terahertz range, *Appl. Phys. A Mater. Sci. Process.* 119(2), 467 (2015)